Coordinated Frequency Control Scheme of Offshore Wind Farm Connected to VSC-HVDC

LIU Xiaoge[a], Zhao XU[a]

[a] *The Department of Electrical Engineering, The Hong Kong Polytechnic University, Kowloon, Hong Kong SAR, People's Republic of China*

E-mail: liuxiaoge07@gmail.com, eezhaoxu@polyu.edu.hk

Coordinated Frequency Control Scheme of Offshore Wind Farm Connected to VSC-HVDC

LIU Xiaoge[a], Zhao XU[a]

[a]*Department of Electrical Engineering, The Hong Kong Polytechnic University, Hong Kong SAR, China.*
E-mail: liuxiaoge07@gmail.com, eezhaoxu@polyu.edu.hk

Abstract: This paper presents a coordinated control scheme enabling the VSC-HVDC connected offshore wind farm to provide frequency response. Once the onshore system frequency deviates, the proposed control strategy will be activated so that both the wind farm and the VSC-HVDC can work together to provide frequency support. In this approach, each wind turbine should operate in de-loading mode to acquire reserve under normal condition. On detecting the frequency event, not only the reserve and kinetic energy of each wind turbine can be utilized for frequency regulation by adjusting rotor speed, but the DC capacitor installed in the VSC-HVDC is arranged to participate in frequency control by slightly changing the DC-link voltage as well. The superior performance of the proposed control method has been verified by simulation.

Keywords: Variable speed wind turbine, offshore wind farm, high voltage direct current, primary frequency control, emulated inertia control

1 Introduction

The integration of offshore wind power plants (OWPPs) connected to voltage source converter based high voltage direct current transmission (VSC-HVDC) system increases continuously during recent years [1]. However, the application of these VSC-HVDC connected OWPPs may compromise onshore system frequency. Firstly, the uncertainty of the wind speed may lead to power imbalance, and thus the frequency may

fluctuate [2]. Secondly, the rotor speed of each wind turbine is no longer associated with system frequency due to the installation of converters [3]. As a result, the inertia of future power system may reduce so that the power system may become more vulnerable to disturbances [4].

To address the technical challenges imposed by the VSC-HVDC connected OWPPs, it may be necessary to explore the capability of the OWPPs and VSC-HVDC system for frequency regulation [5]. References [6] and [7] propose that the DC capacitor in the VSC-HVDC system can perform emulated inertia control (EIC) by changing the DC-link voltage. The control schemes designed in these papers can utilize the energy stored in the DC capacitor to realize EIC so that the transient performance of onshore system frequency can be improved.

Apart from the DC capacitor in VSC-HVDC, the wind turbines in OWPPs can also be arranged to participate in frequency control. Up to now, various frequency control strategies applied in wind turbines have been proposed. These control methods can be categorized into two groups: EIC and de-loading operation based primary frequency control (DOPFC) [8], [9].

As mentioned before, the transient behavior of frequency can become better if EIC is performed by the DC capacitor in VSC-HVDC system. Moreover, references [10-12] recommend that frequency derivative controller can be used in each wind turbine to realize EIC. If such controller is applied, the kinetic energy stored in rotor can be extracted to provide virtual inertia support.

The DOPFC strategy aims to utilize the primary reserve acquired from de-loading operation for frequency control. To obtain the power reserve under normal condition, each

wind turbine should operate in de-loading mode and the extracted power is not maximized [2], [8], [13-15]. The power reserve obtained from de-loaded wind turbines may be necessary for future power grids, especially if the penetration level of wind and other renewable energy becomes so high that the traditional resources of reserve may be exhausted. It is inevitable that the wind turbines operating in de-loading mode cannot capture maximum power from wind. Some papers propose that the electricity market mechanism can be modified to compensate the revenue loss of each OWPP [9], [16].

On detecting frequency deviation, the power reserve should be deployed for frequency regulation. References [2], [8], [14], [15], [17] propose that the conventional DOPFC can be achieved by adding an active power reference produced by a frequency proportional controller, but it seems that the mechanical power is not explicitly considered in these control schemes [13]. As a result, it is doubtful that whether the power reserve can be utilized successfully when frequency deviates [12], [13], [18]. The study in [13] suggests that the DOPFC can be realized by controlling pitch angle. However, the adjustment of pitch angle may lead to mechanical fatigue [15]. In [19], a rotor speed closed-loop based frequency regulation strategy involving the adjustment of mechanical power is presented, but the usage of the kinetic energy for frequency response enhancement can be discussed further.

For the VSC-HVDC connected offshore wind farm, not only the energy stored in DC capacitor can be used for frequency control, but the power reserve acquired from de-loading operation and the kinetic energy preserved in rotor can be utilized for frequency regulation as well. Based on the research mentioned above, some coordinated frequency control strategies for VSC-HVDC connected offshore wind farm have been discussed in

[3], [5], [20-31]. The control methods designed in [3], [23], [25-27] focus on the virtual inertia support provided by the VSC-HVDC connected OWPP. In these papers, the wind turbines are arranged to realize EIC. It seems that the application of DOPFC is not concerned. For the coordinated control schemes described in [5], [20-22], [24], [28-31], the conventional DOPFC without considering the mechanical power variation is implemented in each wind turbine. These control methods may not change the mechanical power explicitly [12], [13], [18]. Consequently, the power reserve may not be utilized during frequency excursion, and the potential capability of the OWPP may not be fully exploited.

In this paper, a coordinated frequency control scheme aiming at utilizing the self-capability of the wind turbines and the VSC-HVDC system to provide frequency support is proposed. To enable the wind turbines to perform frequency control, an extended rotor speed control considering the mechanical power variation is designed. Such control strategy can adjust the rotor speed according to frequency deviation. In this way, both the power reserve obtained from de-loading operation and the kinetic energy preserved in rotor can be employed for frequency regulation. Besides, a modified DC-link voltage control is applied to change the voltage of DC capacitor so that the DC capacitor installed in VSC-HVDC system can make use of the stored energy to provide additional frequency response. After being subjected to the disturbances, both the extended rotor speed control and the modified DC-link voltage control will be triggered simultaneously. Consequently, the potential of the VSC-HVDC system and the OWPP can be exerted as much as possible to improve system frequency performance. The simulation results prove that the frequency behavior can become better if the proposed control method is implemented.

The organization of the paper is listed as follows: Section 2 describes the model used in this research. The proposed control scheme is presented in Section 3. The simulation results are provided in Section 4 and main conclusions are summarized in Section 5.

2 System Model for Study

2.1 Overview of The Studied System

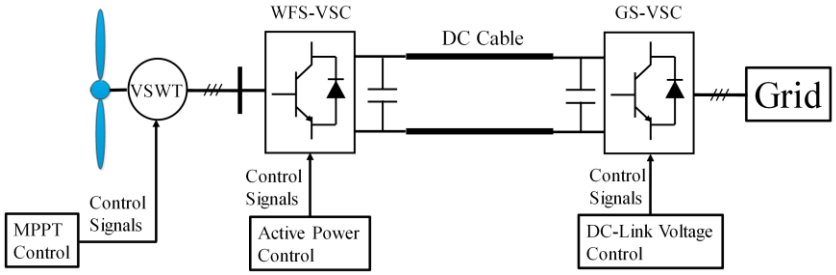

Figure.1 Typical layout of an offshore wind farm connected to a VSC-HVDC transmission system

Figure.1 shows a typical configuration of a VSC-HVDC connected offshore wind farm. In this study, the wind power plant consists of 50 PMSG based wind turbines (PMSG-WTs). The wind farm side voltage source converter (WFS-VSC) of the VSC-HVDC system is used to collect the power generated by the wind turbines, and the grid side voltage source converter (GS-VSC) can transmit the active power to the onshore utility network by stabilizing the DC-link voltage.

2.2 Model and Conventional Control of Wind Turbine

Based on the analysis of wind turbine aerodynamics, the mechanical power of the PMSG-WT can be derived from the following equations [32]:

$$P_m = 0.5C_p(\lambda,\beta)\rho\pi R^2 V_w^3 \tag{1}$$

$$C_p = 0.5176\left(\frac{116}{\gamma} - 0.4\beta - 5\right)e^{-\frac{21}{\gamma}} + 0.0068\lambda \tag{2}$$

$$\gamma = 1/(\frac{1}{\lambda + 0.08\beta} - \frac{0.035}{\beta^3 + 1}) \tag{3}$$

where C_P is power coefficient; λ is tip speed ratio (TSR); β is pitch angle; ρ is air density; R is the radius of the blade; V_w is wind speed.

Traditionally, each wind turbine operates in MPPT mode and extracts maximum power from wind. So far, two methods to realize MPPT operation have been developed in [33]. In this study, a typical MPPT control scheme depicted in Figure. 2 is applied. In this figure, $\omega_{r.ref}$ is the rotor speed reference, λ_{opt} is the optimal TSR where the maximum power can be captured, ω_r is the actual value of rotor speed and $P_{e.ref}$ is the setting-point of active power. The MPPT control is usually implemented in rotor-side converter (RSC). The grid-side converter (GSC) is arranged to maintain the stability of DC-link voltage. In this research, the model of the two converters is established according to the description in [34-36].

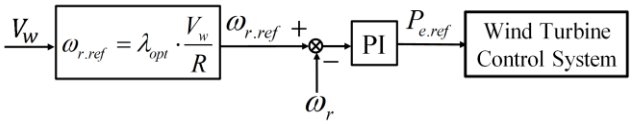

Figure.2 A typical MPPT control method used in this research

As investigated in [34], [35], [37], a two-mass model is accurate enough to describe the dynamic performance of the drive train system. The two-mass model can be represented as follows:

$$T_m = \frac{0.5\rho\pi R^2 C_p(\lambda,\beta)V_W^3}{\omega_t} \tag{4}$$

$$\frac{d\omega_t}{dt} = \frac{1}{2H_t}(T_m - T_{sh}) \tag{5}$$

$$\frac{d\theta_t}{dt} = \omega_b(\omega_t - \omega_r) \tag{6}$$

$$\frac{d\omega_r}{dt} = \frac{1}{2H_g}(T_{sh} - T_e - B\omega_r) \tag{7}$$

$$T_{sh} = K_{sh}\theta_t + D_{sh}\omega_b(\omega_t - \omega_r) \tag{8}$$

where T_m is mechanical torque, ω_t is the turbine speed of each PMSG-WT; T_{sh} is shaft torque; H_t is the inertia constant of turbine; θ_t is shaft twist angle, ω_b is the base value of rotating speed; H_g is the inertia constant of generator, B is friction coefficient, K_{sh} is stiffness constant and D_{sh} is mutual damping.

Figure. 3 presents the pitch angle control system applied in the wind turbine. Such model is based on the description in [38]. Pitch angle controller is installed to limit the rotor speed, especially when wind speed is too high. If the rotor speed exceeds its constraints, the pitch angle controller will be triggered so that the over-speeding operation can be avoided. In this figure, $\omega_{r.max}$ is the maximum rotor speed, β_{opt} is the pitch angle value used for MPPT control, β_{max} is the upper limit of the pitch angle, β_{min} is the minimum value of pitch angle, T_{servo} is the time constant of the servo and k_i is the parameter.

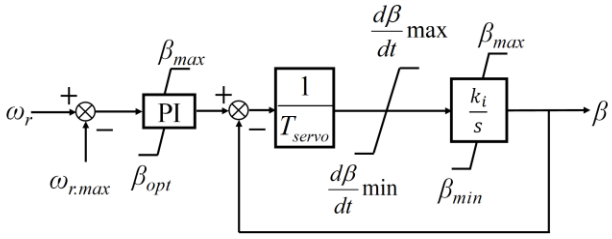

Figure.3 Pitch angle controller in the wind turbine

3 Proposed Frequency Control Scheme for VSC-HVDC Connected Offshore Wind Farm

3.1 Overview of Proposed Control Scheme

If frequency is normal, the wind turbines should operate in de-loading mode instead

of MPPT mode. In this way, the power extracted from wind will not be maximized so that power reserve can be acquired. The de-loading operation can be realized through various methods, such as by adjusting pitch angle or varying rotor speed [15]. In this research, an over-speeding technique is used to implement de-loading operation. Further discussion on over-speeding technique based de-loading operation of wind turbine is provided in Section 3.2.

Figure.4 provides an overview of the proposed frequency control scheme. As soon as the frequency deviation is detected, the extended rotor speed control will be activated so that the reserve acquired from de-loading operation and kinetic energy kept by each wind turbine can be deployed to perform frequency control. Meanwhile, the modified DC-link voltage control can be triggered to exert the energy preserved in the DC capacitors for frequency support provision.

If the extended rotor speed control is implemented, the wind turbine is able to operate at the speed where de-loading operation is achieved under normal condition. When frequency drops, the wind turbine will be driven to a new operating point with a higher power coefficient. As a result, more power can be captured, and thus the active power produced by the wind turbine can increase. In this way, the power reserve kept in advance is employed for frequency regulation. If an over-frequency event occurs, the wind turbine will evolve towards the operating point where less power can be extracted.

By applying the modified DC-link voltage control, the voltage of DC capacitor can be altered so that the VSC-HVDC system can provide additional frequency support. Detailed analysis on such control scheme is carried out in Section 3.4.

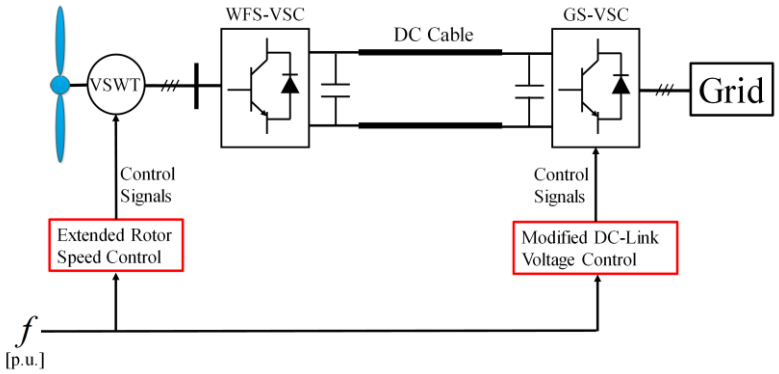

Figure.4 Overview of proposed frequency control scheme

3.2 De-loading Operation of Individual Variable Speed Wind Turbine

In order to quantify the power reserve acquired from de-loading operation, de-loading level $DL_{del.N}$ is defined in [39]. Under normal condition, the definition of $DL_{del.N}$ can be expressed as follows:

$$\begin{aligned} DL_{del.N} &= \frac{P_m^{MPPT} - P_m^{del.N}}{P_m^{MPPT}} \times 100\% \\ &= \frac{0.5C_p^{\max}\rho\pi R^2 V_W^3 - 0.5C_p^{del.N}\rho\pi R^2 V_W^3}{0.5C_p^{\max}\rho\pi R^2 V_W^3} \times 100\% \\ &= \frac{C_p^{\max} - C_p^{del.N}}{C_p^{\max}} \times 100\% \end{aligned} \tag{9}$$

where P_m^{MPPT} is the available power under a certain wind speed, $P_m^{del.N}$ is the extracted power if the wind turbine is de-loaded, C_P^{max} is the maximum power coefficient, $C_P^{del.N}$ is a sub-optimal power coefficient under de-loading operation. From (9), it can be learned that the MPPT operation indicates that the value of $DL_{del.N}$ is zero. Besides, we can acquire the following equation:

$$P_m^{del.N} = P_m^{MPPT}(1 - DL_{del.N}) \tag{10}$$

As mentioned in Section 3.1, either pitch angle or rotor speed can be utilized to realize de-loading operation. Considering that the actuation of pitch angle may lead to

mechanical fatigue, the de-loading operation achieved by adjusting rotor speed is preferred [15].

Figure.5 displays the mapping from λ to power coefficient C_P. Under a certain wind speed, the maximum power can be captured if the wind turbine rotates at the speed determined by the optimal tip speed ratio λ_{opt}, while $C_P^{del.N}$ can be achieved by operating at the speed determined by a lower-than-optimal TSR $\lambda_{del.N}^{US}$ or a higher-than-optimal TSR $\lambda_{del.N}^{OS}$. Furthermore, either under-speeding technique or over-speeding technique can be considered to realize de-loading operation [2], [40], [41]. In this research, the over-speeding technique is selected for de-loading operation, as the additional kinetic energy can be stored by using such approach [41].

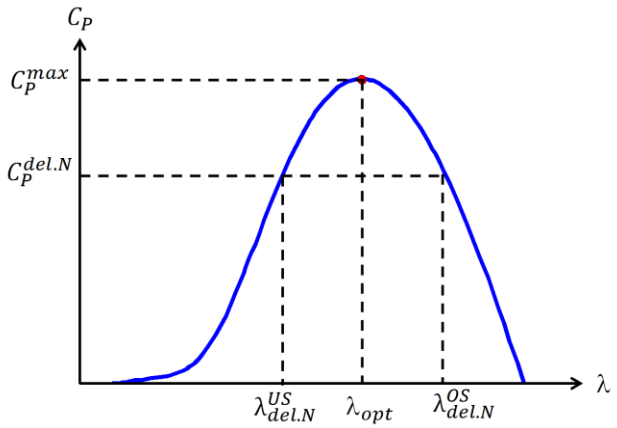

Figure.5 The relationship between tip speed ratio λ and power coefficient C_P

To implement the over-speeding technique, the control scheme shown in Figure.6 should be applied. According to this figure, if the desired de-loading level is given, the corresponding $C_P^{del.N}$ can be calculated from the wind turbine characteristics. Based on the value of $C_P^{del.N}$ and the relationship between C_P and λ, the rotor speed reference for de-loading operation can be obtained.

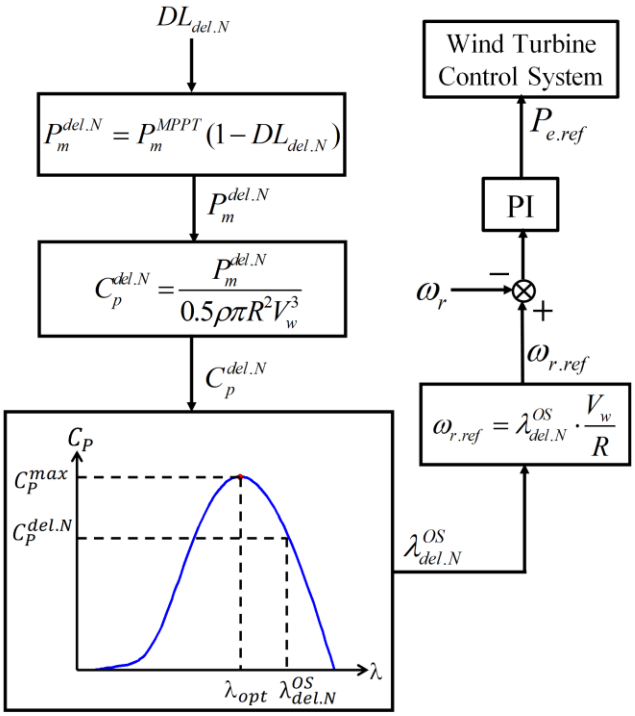

Figure.6 Rotor speed control scheme for de-loading operation

3.3 Extended Rotor Speed Control of each VSWT

To utilize the power reserve for frequency regulation, the turbine speed should be adjusted so that the mechanical power captured by the blades can be varied with onshore system frequency. Furthermore, the captured power should increase if an under-frequency event occurs, while less power should be extracted when frequency rises.

In this section, an extended rotor speed control scheme is described. Compared to the rotor speed control method shown in [19], a frequency derivative (D) controller is inserted in the extended rotor speed control strategy presented in Figure.7. Hence, the energy stored in rotor can be exploited to enhance the emulated inertia support.

In Figure.7, f_N is the normal value of frequency, while f is the actual system frequency. $P_m^{del.f}$ represents the required mechanical power in real-time. We can notice that the $P_m^{del.f}$ can be obtained by adding $P_m^{del.N}$ to the output of the frequency proportional (P)

controller. In this controller, K_P is the parameter. The discussion about the K_P selection is provided in Section 4. If the $P_m^{del.f}$ is given, the corresponding power coefficient $C_P^{del.f}$ and $\lambda_{del.f}^{OS}$ can be acquired from (1) and the $C_P - \lambda$ characteristics. After $\lambda_{del.f}^{OS}$ is determined, the desirable rotor speed reference $\omega_{r.ref}$ can be generated. Then the rotor speed controller will bring the wind turbine to operate at a new equilibrium point. As a result, the mechanical power can be adjusted and the power reserve can be deployed.

Apparently, wind speed information is necessary for the implementation of the extended rotor speed control. To measure the wind speed in practice, the light detection and ranging (LIDAR) system described in [42] can be installed in each wind turbine. Moreover, the pitch angle control system will be activated if wind speed is too high. The frequency support provided by the pitch angle control system will be evaluated in the immediate future.

Owing to the variation of the rotor speed, not only the mechanical power can be altered for frequency control, but the kinetic energy can be exploited to improve the frequency performance as well. The frequency D controller can produce a compensating item so that the kinetic energy can be employed to perform emulated inertia control. Besides, it is noteworthy that the drive train system in each wind turbine may cause torsion oscillation, and therefore the onshore system frequency may fluctuate in practice [37]. If the frequency D controller is applied, such frequency fluctuation can be mitigated.

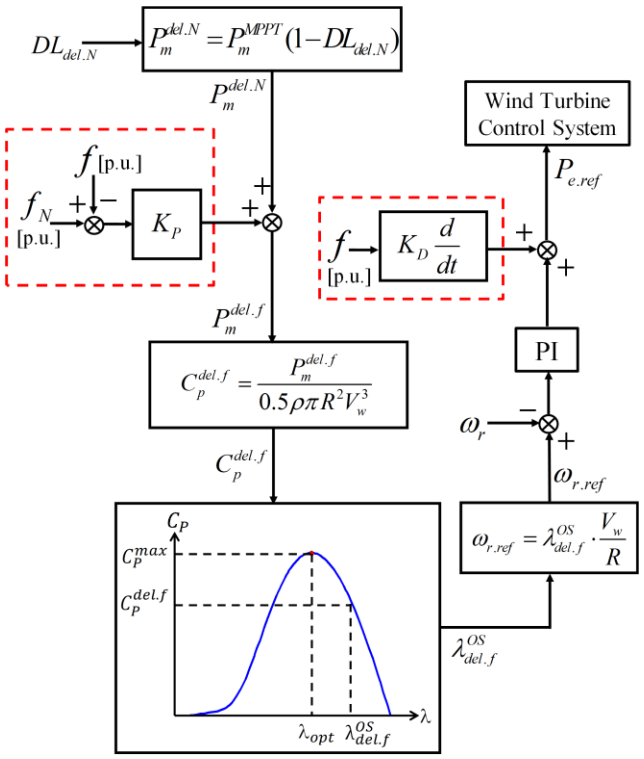

Figure.7 Extended rotor speed control scheme for frequency regulation

3.4 Modified DC-link Voltage Control for VSC-HVDC

Conventionally, the DC-link voltage in a VSC-HVDC system should remain constant. In this way, the power generated by the wind turbines can be delivered to the main grid. As discussed in [6] and [7], the energy stored in the DC capacitor can be deployed to provide additional virtual inertia support by modifying the DC-link voltage control strategy. The modified DC-link voltage control approach can be developed from the frequency D controller shown as follows [7]:

$$P_{e.hvdc} = U_{DC.hvdc} \cdot C_{DC.hvdc} \frac{dU_{DC.hvdc}}{dt} = K_{D.hvdc} \cdot \frac{df}{dt} \tag{11}$$

where $P_{e.hvdc}$ is the active power provided by the DC capacitor, $U_{DC.hvdc}$ is the value of DC-link voltage and $C_{DC.hvdc}$ is the capacitance. $K_{D.hvdc}$ is the parameter of the D controller, f is the frequency of the onshore power system. Then by using the Newton-

Leibniz formula, we can obtain that:

$$\begin{aligned}&\int_{t_0}^{t} P_{e.hvdc}\cdot dt=\int_{U_{DC.hvdc.N}}^{U_{DC.hvdc}} U_{DC.hvdc}\cdot C_{DC.hvdc}\cdot dU_{DC.hvdc}\\&=\int_{f_N}^{f} K_{D.hvdc}\cdot f\cdot df\end{aligned} \tag{12}$$

where $U_{DC.hvdc.N}$ is the normal value of DC-link voltage. Furthermore, the following equations can be acquired:

$$\frac{1}{2}C_{DC.hvdc}\left(U_{DC.hvdc}^{2}-U_{DC.hvdc.N}^{2}\right)=\frac{1}{2}K_{D.hvdc}(f^{2}-f_N^{2}) \tag{13}$$

$$\frac{1}{2}C_{DC.hvdc}\left[\left(U_{DC.hvdc.N}+\Delta U_{DC.hvdc}\right)^{2}\text{-}U_{DC.hvdc.N}^{2}\right]=\frac{1}{2}K_{D.hvdc}\left[\left(f_N+\Delta f\right)^{2}-f_N^{2}\right] \tag{14}$$

in which $\Delta U_{DC.hvdc}$ and Δf denote the DC-link voltage variation and frequency variation respectively. Compared to $U_{DC.hvdc.N}$ and f_N, $\Delta U_{DC.hvdc}$ and Δf can be regarded as small values. Hence, the higher order terms such as $\Delta U_{DC.hvdc}^{2}$ and Δf^{2} can be excluded and the simplified formulas can be expressed as:

$$C_{DC.hvdc}\cdot U_{DC.hvdc.N}\cdot\Delta U_{DC.hvdc}=K_{D.hvdc}\cdot f_N\cdot\Delta f \tag{15}$$

$$C_{DC.hvdc}\cdot U_{DC.hvdc.N}\cdot\left(U_{DC.hvdc}-U_{DC.hvdc.N}\right)=K_{D.hvdc}\cdot f_N\cdot(f-f_N) \tag{16}$$

Considering that (16) is derived from (11), it can be learnt that the DC capacitor can provide virtual inertia support if the setting-point of DC-link voltage can be varied with the onshore system frequency. The relationship between $U_{DC.hvdc}$ and f can be described as:

$$U_{DC.hvdc}=K_{P.hvdc}\cdot(f-f_N)+U_{DC.hvdc.N} \tag{17}$$

where $K_{P.hvdc}$ is the gain which can be calculated by the following equation:

$$K_{P.hvdc}=\frac{K_{D.hvdc}\cdot f_N}{C_{DC.hvdc}\cdot U_{DC.hvdc.N}} \tag{18}$$

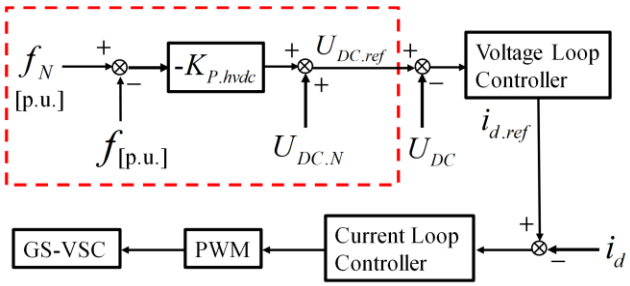

Figure.8 Modified DC-link voltage control scheme for frequency regulation

Figure.8 shows the modified DC-link voltage control scheme which is acquired from (17). In this figure, U_{DC} is the actual value of DC-link voltage, $i_{d.ref}$ is the reference of d-axis component of current, and i_d is the actual value of the current component in d-axis. Compared to the conventional DC-link voltage controller in which the $U_{DC.ref}$ is fixed, the $U_{DC.ref}$ applied in the modified DC-link voltage controller can be adjusted according to frequency deviation. Such controller can boost the DC-link voltage if an over-frequency event occurs so that the surplus active power can be stored. In addition, the voltage of the DC capacitor will decrease when frequency falls, and thus the energy can be released to the power grid. It should be noted that the bound of DC-link voltage is associated with the value of $K_{P.hvdc}$. The setting of $K_{P.hvdc}$ is briefly discussed in Section.4.

4 Simulation Results

Figure. 9 shows the power system established for simulation study. As depicted in this figure, the wind farm consisting of 50 wind turbines is connected to the onshore system via VSC-HVDC link. Besides, two thermal power plants are installed in the main grid. The nominal frequency of the onshore system is 50 Hz. As discussed in [43], the damping coefficient of load is set as 1.5 in this paper. The description of the two thermal power plants can be found in [44]. The parameters used in this power system are provided in Appendix.

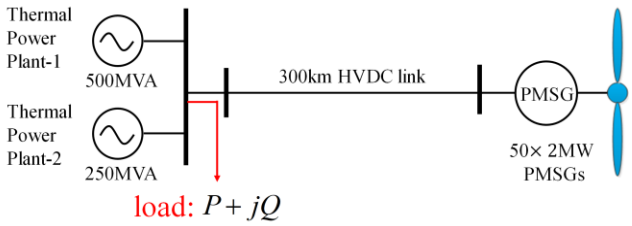

Figure.9 Configuration of the studied power system

The control schemes applied for comparison are listed as follows:

Scheme A: The wind turbines are arranged to operate in MPPT mode and the VSC-HVDC system does not provide any frequency response.

Scheme B: Only the wind turbines installed in the wind farm participate in frequency control.

Scheme C: Both the wind turbines and the VSC-HVDC system provide frequency support.

In this paper, the $DL_{del.N}$ is predetermined and the value is set as 10% herein, as we emphasize how to utilize the power reserve kept by each wind turbine for frequency regulation. The parameter K_P can be given by:

$$K_P = \frac{P_m^{MPPT} - P_m^{del.N}}{f_N - f_{min}^{WT}} \times f_N \tag{19}$$

In (19), f_{min}^{WT} represents the frequency under which the wind turbine can operate in MPPT points. Such K_P value is also implemented in the event of an over-frequency incident. In this simulation, f_{min}^{WT} is 49.8Hz.

As mentioned before, (17) indicates that $K_{P.hvdc}$ is related to the range of DC-link voltage, the value of $K_{P.hvdc}$ can be acquired from the following equation:

$$K_{P.hvdc} = \frac{U_{DC.hvdc.N} - U_{DC.hvdc.\min}}{f_N - f_{\min}^{hvdc}} \times f_N \tag{20}$$

where f_{min}^{hvdc} is the frequency value when the DC-link voltage reaches its lower limit $U_{DC.hvdc.min}$. Similarly, the $K_{P.hvdc}$ calculated by (20) is also applied in the proposed control scheme if frequency rises. In this test, the f_{min}^{hvdc} is set as 49.8 Hz and $U_{DC.hvdc.min}$ is set as 0.85 p.u.. Further investigation of these control parameters will be conducted in the future.

In Section 4.1 and 4.2, the simulation study under constant wind speed is carried out. It is noteworthy that the comparison of different DOPFC strategies is provided in Section 4.1.1. In order to assess the frequency response, the rate of change of frequency (ROCOF), the frequency nadir f_{nadir} and the final value of frequency f_{final} are used. In this study, f_{nadir} is defined as the frequency value obtained when maximum frequency deviation is achieved. Furthermore, the lowest frequency value can be regarded as f_{nadir} when frequency falls. If an over-frequency event occurs, the f_{nadir} represents the peak value of system frequency. The maximum absolute value of ROCOF and f_{nadir} can be used to evaluate the transient behavior of system frequency, while the f_{final} can roughly describe the steady-state frequency.

The simulation test under variable wind speed is performed in Section 4.3. To evaluate the performance of onshore system frequency, the mean value of $|\Delta f|$, which is computed by averaging the absolute value of frequency error Δf, and f_{nadir} are recorded.

4.1 Under-frequency Event Under Constant Wind Speed

Case. A: If the wind speed is 8m/s, an under-frequency event occurs at 40s, because load increases by (75+j7.5) MVA.

4.1.1 Performance of Different DOPFC Strategies under Case. A

Conventionally, the DOPFC is realized by adding an active power compensating

item produced by a frequency proportional controller. The conventional DOPFC can be described as follows:

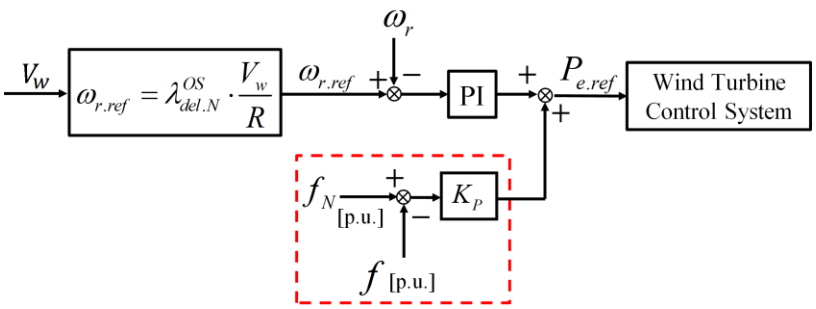

Figure. 10 Conventional DOPFC scheme

To validate the effectiveness of the extended rotor speed control scheme, the following DOPFC schemes are used for comparison:

***DOPFC A*:** conventional DOPFC scheme presented in Figure. 10;

***DOPFC B*:** proposed extended rotor speed control without frequency derivative controller shown in Figure. 7;

***DOPFC C*:** proposed extended rotor speed control with frequency derivative controller shown in Figure.7;

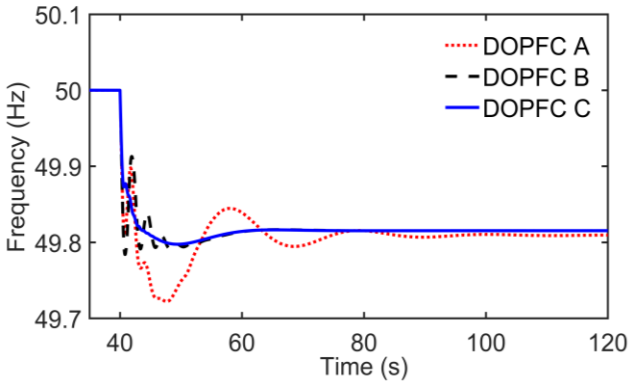

a

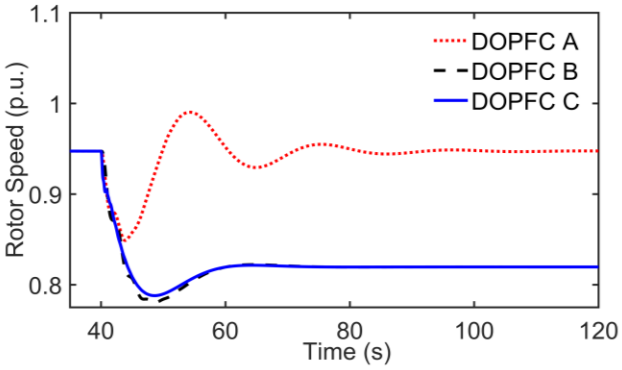

b

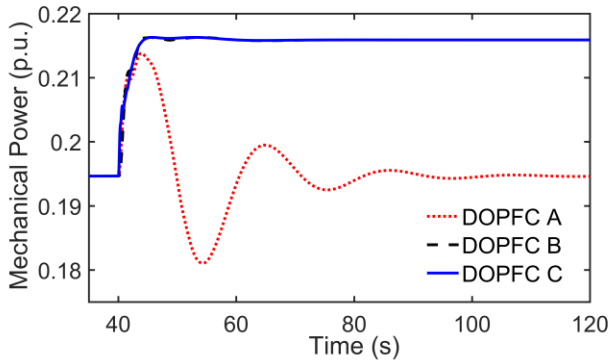

c

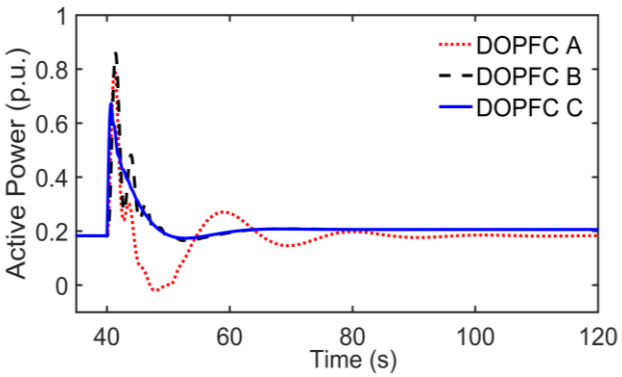

d

Figure.11 Performance of different DOPFC schemes under Case. A

(a) variation of system frequency, (b) variation of rotor speed, (c) variation of mechanical power, (d) variation of active power injected into the main grid

Table 1 Frequency performance of different DOPFC schemes under Case. A

Schemes	Maximum |ROCOF| (Hz/s)	f_{nadir} (Hz)	f_{final} (Hz)
DOPFC A	0.3639	49.7218	49.8093
DOPFC B	0.3766	49.7839	49.8152
DOPFC C	0.3352	49.7973	49.8152

Table 2 Wind turbine performance of different DOPFC schemes under Case. A

Schemes	Initial Value of ω_r (p.u.)	Final Value of ω_r (p.u.)	Initial Value of P_m (p.u.)	Final Value of P_m (p.u.)
DOPFC A	0.9473	0.9472	0.1947	0.1947
DOPFC B	0.9473	0.8195	0.1947	0.2159
DOPFC C	0.9473	0.8195	0.1947	0.2159

The performance of different DOPFC schemes under Case. A is shown in Figure. 11. The data describing system frequency behavior and individual wind turbine performance are recorded in Table 1 and Table 2. Under normal condition, the wind turbines are arranged to operate in de-loading mode and the corresponding rotor speed is 0.9473 p.u., which is higher than the optimal value 0.8 p.u.. From the results, we can learn that the wind turbine with DOPFC A cannot move toward to the optimal rotor speed (0.8 p.u.) where the maximum power can be captured. Because the rotor speed reference in DOPFC A is fixed, the rotor speed closed-loop controller will force the wind turbine to operate at the de-loading operation point (0.9473 p.u.) finally, and thus the power extracted from wind is still 0.1947 p.u.. As a result, the power reserve obtained from de-loading operation is not released in this case.

However, the variation of mechanical power is considered in DOPFC B and DOPFC C. Since the rotor speed reference generated by DOPFC B or DOPFC C can be varied according to the frequency deviation, the wind turbine can approach to the optimal rotor

speed so that more power can be captured. As a result, the power reserve can be utilized for frequency regulation and f_{final} can be improved to 49.8152 Hz. It is noteworthy that if DOPFC B is applied, the system frequency may fluctuate significantly due to the torsional oscillation. Such fluctuation can be mitigated if DOPFC C is applied, for a frequency derivative controller is included.

4.1.2 Effectiveness of Proposed Coordinated Frequency Control Schemes

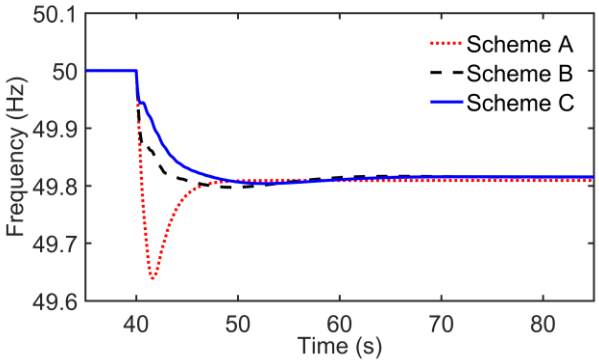

a

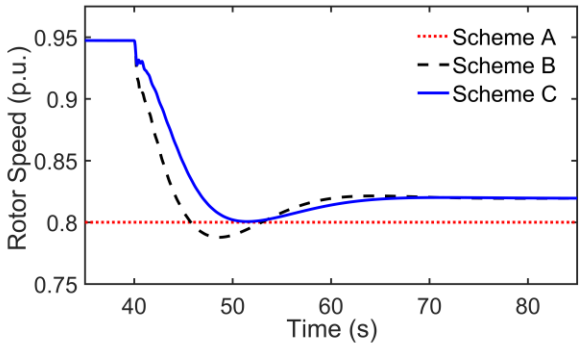

b

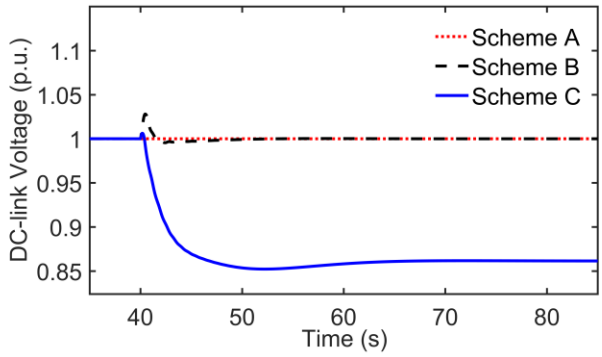

c

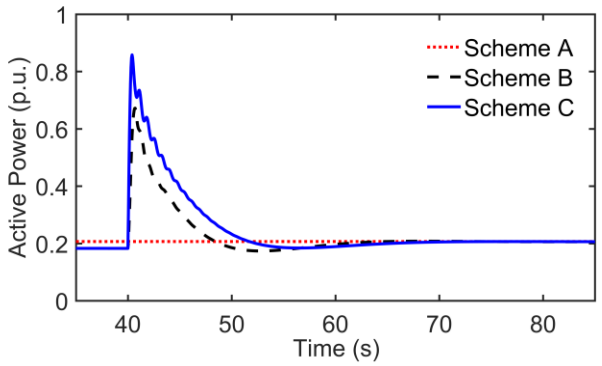

d

Figure. 12 Simulation results of Case. A

(a) variation of system frequency, (b) variation of rotor speed, (c) variation of DC-link voltage, (d) variation of active power injected into the main grid

Table 3 Frequency performance of Case. A

Schemes	Maximum |ROCOF| (Hz/s)	f_{nadir} (Hz)	f_{final} (Hz)
Scheme A	0.3875	49.6393	49.8093
Scheme B	0.3352	49.7973	49.8152
Scheme C	0.3046	49.8039	49.8152

Table 4 Wind turbine performance of Case. A

Schemes	Initial Value of ω_r (p.u.)	Final Value of ω_r (p.u.)	Initial Value of P_m (p.u.)	Final Value of P_m (p.u.)
Scheme A	0.8	0.8	0.2163	0.2163
Scheme B	0.9473	0.8195	0.1947	0.2159
Scheme C	0.9473	0.8195	0.1947	0.2159

Figure. 12 shows the simulation results of Case. A. Relevant data are listed in Table 3 and Table 4. Under normal condition, the wind turbines with Scheme B or Scheme C operate in de-loading mode and thus these wind turbines rotate at a speed of 0.9473 p.u., which is higher than the optimal speed 0.8 p.u..

From Table 3 and Table 4, we can learn that without frequency control strategy, the rotor speed of each wind turbine remains at 0.8p.u..Hence, such wind turbines do not react to the frequency event. However, if Scheme B or Scheme C is applied, the maximum $|ROCOF|$ will reduce significantly and f_{nadir} can be improved. f_{final} also increases from 49.8093 Hz to 49.8152 Hz, because the reserve is deployed and more power is extracted from wind. Moreover, owing to the usage of DC capacitor in Scheme C, the fall of system frequency results in the decrease of DC-link voltage so that the energy stored in DC capacitor is released to provide additional emulated inertia support. Hence, the maximum $|ROCOF|$ can become smaller and f_{nadir} can be improved further.

4.2 Over-frequency Event Under Constant Wind Speed

Case. B: If the wind speed is 8m/s, an over-frequency event occurs at 40s, because load decreases by (75+j7.5) MVA.

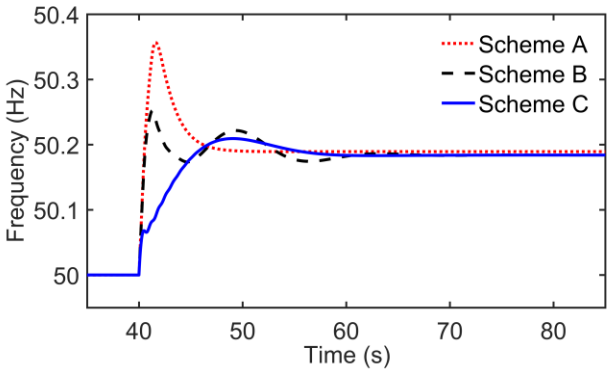

a

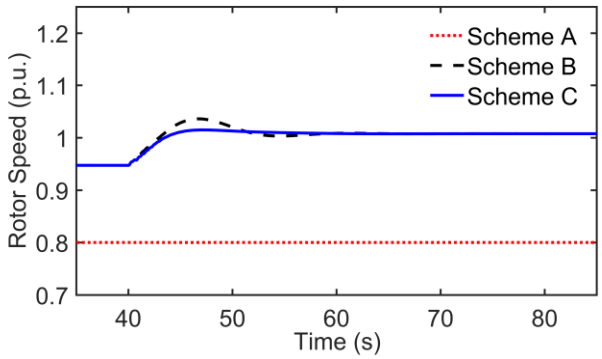

b

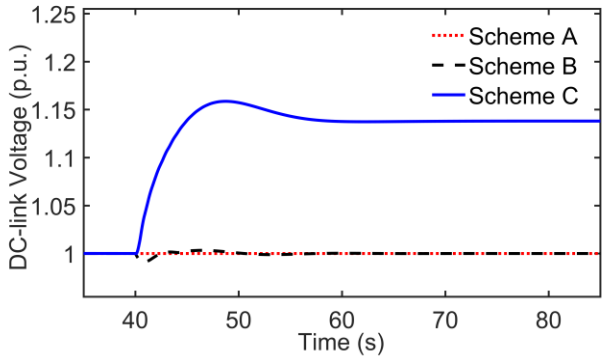

c

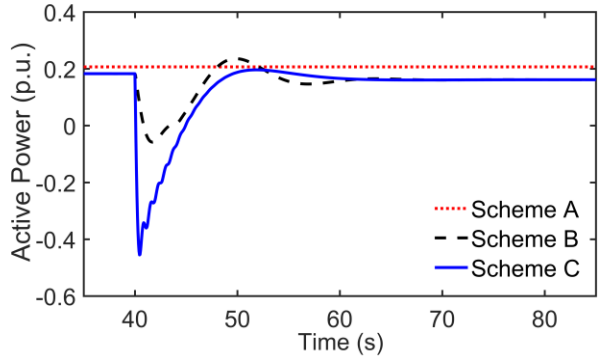

d

Figure. 13 Simulation results of Case. B

(a) variation of system frequency, (b) variation of rotor speed, (c) variation of DC-link voltage, (d) variation of active power injected into the main grid

The frequency performance of Case. B is described in Figure.13 and Table 5.

According to the simulation results, the greatest frequency overshoot and the largest frequency change rate can be acquired if no frequency control scheme is applied. However, as soon as the frequency rise is detected, the wind turbines with Scheme B or Scheme C will speed up so that the additional active power can be stored as kinetic energy. In addition, the extracted mechanical power will decrease due to the acceleration. As a result, the peak value of frequency reduces, and the final value of frequency decreases as well.

Besides, the implementation of Scheme B will not change the DC-link voltage, whereas the Scheme C will exploit the potential of DC capacitor to enhance frequency response. Furthermore, due to the application of Scheme C, the DC-link voltage will increase and absorb the energy to alleviate the power imbalance if the over-frequency event occurs. Consequently, both the frequency change rate and the peak value of frequency can become smaller.

Table 5 Frequency performance of Case. B

Schemes	Maximum |ROCOF| (Hz/s)	f_{nadir} (Hz)	f_{final} (Hz)
Scheme A	0.3818	50.3566	50.1893
Scheme B	0.3539	50.2520	50.1840
Scheme C	0.3108	50.2093	50.1840

Table 6 Wind turbine performance of Case. B

Schemes	Initial Value of ω_r (p.u.)	Final Value of ω_r (p.u.)	Initial Value of P_m (p.u.)	Final Value of P_m (p.u.)
Scheme A	0.8	0.8	0.2163	0.2163
Scheme B	0.9473	1.0078	0.1947	0.1746
Scheme C	0.9473	1.0078	0.1947	0.1746

4.3 Under-frequency Event Under Variable Wind Speed

Case. C If the wind speed is variable, an under-frequency event occurs at 180s, because load increases by (75+j7.5) MVA.

Case. C aims to demonstrate the effectiveness of the proposed control scheme in case of variable wind speed. The wind speed profile for simulation is shown in Figure. 14. The data of the wind speed can be found in [45]. In this case, the load increases suddenly at 180s.

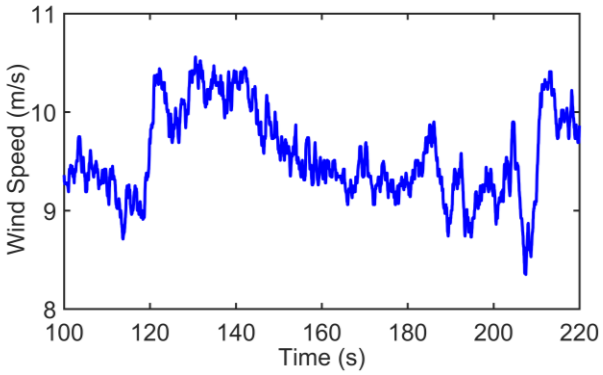

Figure. 14 Variable wind speed profile for Case. C

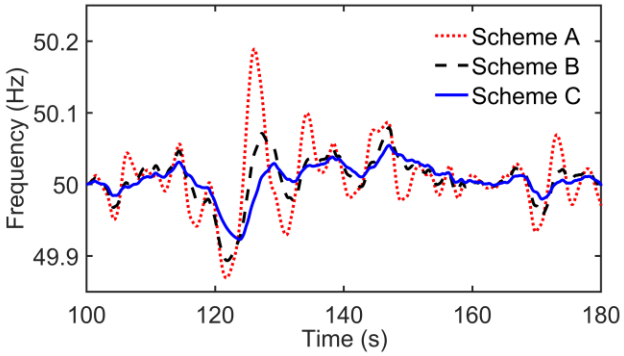

a

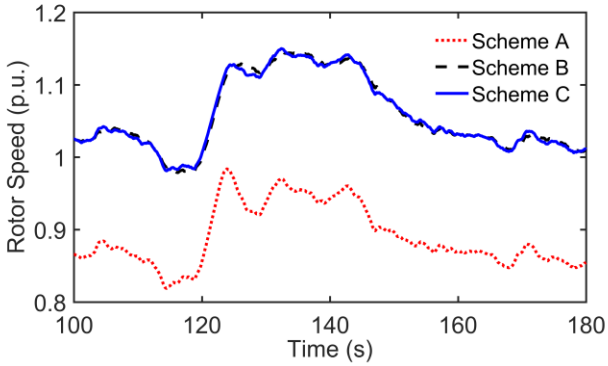

b

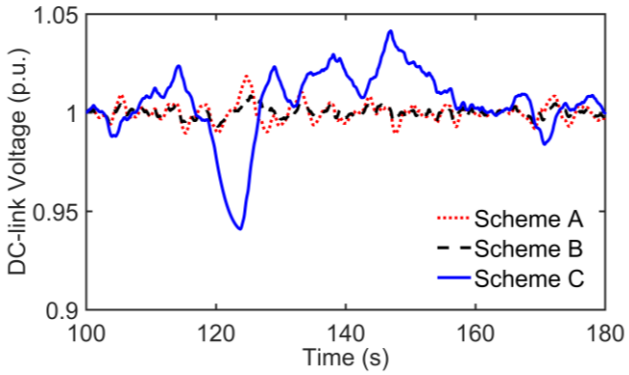

c

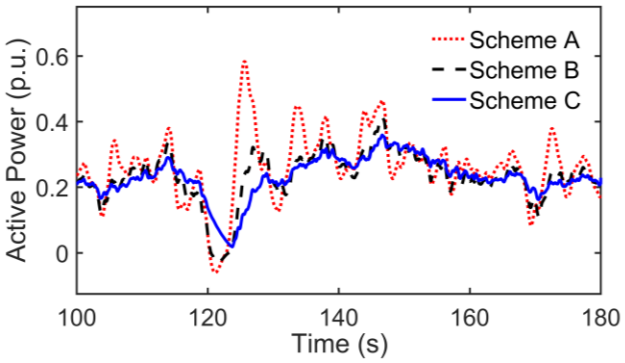

d

Figure. 15. Simulation results of Case. C (100s~180s)

(a) variation of system frequency, (b) variation of rotor speed, (c) variation of DC-link voltage, (d) variation of active power injected into the main grid

Figure. 15 depicts the simulation results describing the performance under constant load. The data assessing the frequency behaviour is shown in Table 7. From the figure, we can observe that under variable wind speed, the power generated by the wind turbines will fluctuate. The power fluctuation can result in the frequency deviation. However, if the Scheme B is triggered and the wind turbines are able to provide frequency response, the mean value of $|\Delta f|$ will be smaller and the frequency curve will become smoother. Furthermore, Scheme C can exploit the energy in DC capacitor to provide additional virtual

inertia support so that the smallest mean value of $|\Delta f|$ and the smoothest frequency curve can be acquired.

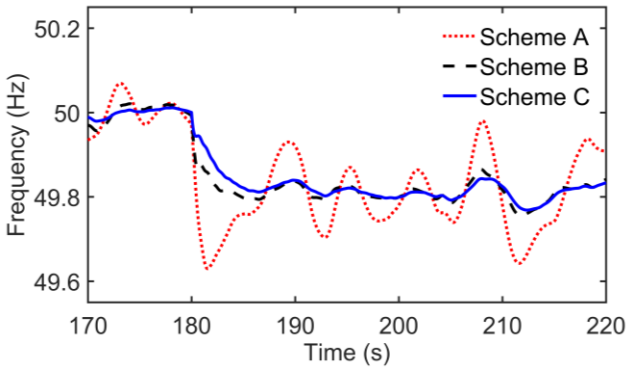

a

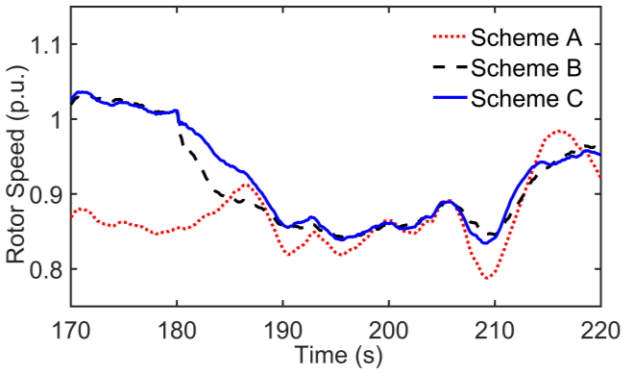

b

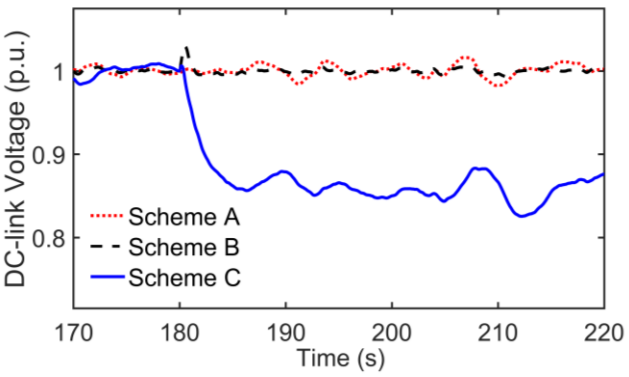

c

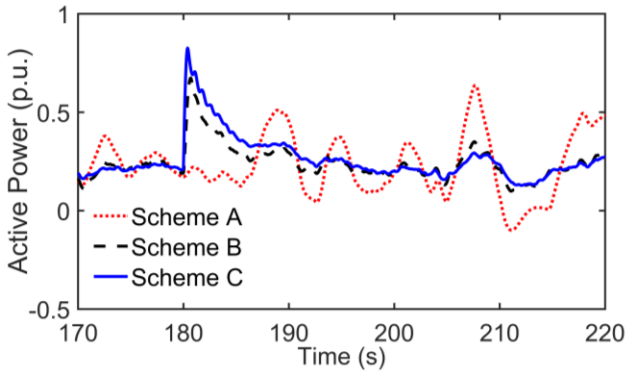

d

Figure. 16. Simulation results of Case. C (170s~220s)

(a) variation of system frequency, (b) variation of rotor speed, (c) variation of DC-link voltage, (d) variation of active power injected into the main grid

Table 7 Frequency performance of Case. C

Schemes	mean value of $\|\Delta f\|$ during 100s~180s (Hz)	f_{nadir} (Hz) during 170s~220s
Scheme A	0.0346	49.6296
Scheme B	0.0243	49.7563
Scheme C	0.0179	49.7686

The frequency behavior of the under-frequency event in Case C is shown in Figure.16, and the values of f_{nadir} are also provided in Table 7. During this event, the lowest frequency nadir can be recorded on condition that no frequency control strategy is implemented. The dynamic frequency performance can be improved if Scheme B or Scheme C is activated. Due to the participation of VSC-HVDC system in frequency control, the Scheme C can lead to the highest value of f_{nadir}.

5 Conclusion and Future Work

In this paper, a frequency control scheme coordinating VSC-HVDC system with offshore wind farm is designed. Such control approach consists of an extended rotor speed control and a modified DC-link voltage control so that the potential of the VSC-HVDC

system and the wind turbines can be exploited as much as possible for frequency response enhancement. By applying the extended rotor speed control, both the power reserve obtained from de-loading operation and the kinetic energy preserved by each wind turbine can be deployed for frequency control. In addition, the DC capacitor installed in the VSC-HVDC system is also able to participate in frequency regulation by varying the DC-link voltage. In this way, the energy stored in the DC capacitor can be utilized to enhance the virtual inertia support further.

The simulation results can prove the effectiveness of the proposed control scheme. The frequency performance can be improved significantly if the extended rotor speed control is activated alone, while the coordinated control strategy can provide additional emulated inertia support so that the behavior of system frequency can become better.

Several technical challenges may be worth investigating in the future. For instance, the determination of the de-loading level under normal condition can be considered. Besides, the offshore wind farm should be aware of the onshore system frequency. Therefore, a reliable mechanism for the offshore wind farm to sense the system frequency variation should be designed in practice. Moreover, the methods to restore the DC-link voltage can be explored in the future as well.

Appendix

(1) Parameters of the wind turbine:
WT: Rated wind speed is 13.33m/s; inertia constant $H_t = 4.32\mathrm{s}$; damping coefficient $D_{sh} = 1.11\mathrm{p.u.}$; shaft stiffness coefficient $K_{sh} = 1.5\mathrm{p.u.}$; time constant of the pitch servo $T_{servo} = 0.01\mathrm{s}$; $\beta_{max} = 27deg$.

PMSG: Rated power is 2MW; inertia constant $H_g = 0.62\mathrm{s}$; friction coefficient $B = 0.01\mathrm{p.u.}$; stator resistance $R_s = 0.006\mathrm{p.u}$, d-axis synchronous reactance (p.u.): x_d=1.305, x'_d=0.296, x''_d=0.252; q-axis synchronous reactance (p.u.): x_q=0.474, x'_q=0.474, x''_q=0.243, $L_g = 0.15p.u.$, $R_g = 0.003p.u.$.

(2) Parameter of excitation system in thermal power plant 1&2:
Regulator gain K_{ES}: 300; time constant T_{ES}: 0.01s.

(3) Parameter of governor in thermal power plant-1:
Servo-motor time constant T_{sm}: 0.025s, gate closing rate $V_{G.MIN}$ -0.1 p.u./s; gate opening rate $V_{G.MAX}$ 0.1 p.u./s; Governor time constants T_2=0s, T_3=0.3s, T_4=4s, T_5=0.1s; Turbine torque fractions F_2=0, F_3=0.3, F_4=0.4, F_5=0.3; droop value R_P=4%.

(4) Parameter of governor in thermal power plant-2:
Servo-motor time constant T_{sm}: 0.025s, gate closing rate $V_{G.MIN}$ -0.1 p.u./s; gate opening rate $V_{G.MAX}$ 0.1 p.u./s; Governor time constants T=0.2s; droop value R_P=4%

(5) Parameter of synchronous generator in thermal power plant-1:
Nominal power 500 MVA; d-axis synchronous reactance: x_d=2.54 p.u., x'_d=0.237 p.u., x''_d=0.183 p.u.; q-axis synchronous reactance x_q=2.31 p.u., x'_q=0.392 p.u., x''_q=0.191 p.u.; inertial contant 5s; friction factor 0.01; stator resistance 0.0021 p.u.

(6) Parameter of synchronous generator in thermal power plant-2:
Nominal power:250 MVA; d-axis synchronous reactance: x_d=2.349 p.u., x'_d=0.219 p.u., x''_d=0.169 p.u.; q-axis synchronous reactance x_q=2.136 p.u., x'_q=0.362 p.u., x''_q=0.177 p.u.; inertial contant 5s; friction factor 0.01; stator resistance 0.002 p.u.

(7) Parameters of VSC-HVDC system:
Rated VSC AC rms voltage:110kV; nominal DC voltage: 200kV; DC capacitance: 20000*uF*; resistance of DC cable: 0.015ohm/km; inductance of DC cable: 0.792mH/km; capacitance of DC cable: 14.4×10^{-9}F/m.

Reference

[1] M. Zhang, X. Yuan, and J. Hu, "Inertia and Primary Frequency Provisions of PLL-Synchronized VSC HVDC When Attached to Islanded AC System," *IEEE Transactions on Power Systems,* vol. 33, no. 4, pp. 4179-4188, 2018.

[2] K. V. Vidyanandan and N. Senroy, "Primary frequency regulation by deloaded wind turbines using variable droop," *IEEE Transactions on Power Systems,* vol. 28, no. 2, pp. 837-846, 2013.

[3] X. Liu and A. Lindemann, "Control of VSC-HVDC Connected Offshore Windfarms for Providing Synthetic Inertia," *IEEE Journal of Emerging and Selected Topics in Power Electronics,* vol. PP, no. 99, pp. 1-1, 2017.

[4] S. Ghosh, S. Kamalasadan, N. Senroy, and J. Enslin, "Doubly Fed Induction Generator (DFIG)-Based Wind Farm Control Framework for Primary Frequency and Inertial Response Application," *IEEE Transactions on Power Systems,* vol. 31, no. 3, pp. 1861-1871, 2016.

[5] P. Kou, D. Liang, Z. Wu, Q. Ze, and L. Gao, "Frequency Support From a DC-Grid Offshore Wind Farm Connected Through HVDC Link: A Communication Free Approach," *IEEE Transactions on Energy Conversion,* 2018.

[6] Y. Phulpin, "Communication-Free Inertia and Frequency Control for Wind Generators Connected by an HVDC-Link," *IEEE Transactions on Power Systems,* vol. 27, no. 2, pp. 1136-1137, 2012.

[7] J. Zhu, C. D. Booth, G. P. Adam, A. J. Roscoe, and C. G. Bright, "Inertia Emulation Control Strategy for VSC-HVDC Transmission Systems," *IEEE Transactions on Power Systems,* vol. 28, no. 2, pp. 1277-1287, 2013.

[8] R. G. d. Almeida and J. A. P. Lopes, "Participation of Doubly Fed Induction Wind Generators in System Frequency Regulation," *IEEE Transactions on Power Systems,* vol. 22, no. 3, pp. 944-950, 2007.

[9] F. Wilches-Bernal, J. H. Chow, and J. J. Sanchez-Gasca, "A Fundamental Study of Applying Wind Turbines for Power System Frequency Control," *IEEE Transactions on Power Systems,* vol. 31, no. 2, pp. 1496-1505, 2016.

[10] J. M. Mauricio, A. Marano, A. Gomez-Exposito, and J. L. M. Ramos, "Frequency Regulation Contribution Through Variable-Speed Wind Energy Conversion Systems," *IEEE Transactions on Power Systems,* vol. 24, no. 1, pp. 173-180, 2009.

[11] M. F. M. Arani and E. F. El-Saadany, "Implementing Virtual Inertia in DFIG-Based Wind Power Generation," *IEEE Transactions on Power Systems,* vol. 28, no. 2, pp. 1373-1384, 2013.

[12] R. Chen, W. Wu, H. Sun, Y. Hu, and B. Zhang, "Supplemental control for enhancing primary frequency response of DFIG-based wind farm considering security of wind turbines," in *2014 IEEE PES General Meeting | Conference & Exposition*, 2014, pp. 1-5.

[13] Y. Fu, Y. Wang, and X. Zhang, "Integrated wind turbine controller with virtual inertia and primary frequency responses for grid dynamic frequency support," *IET Renewable Power Generation,* vol. 11, no. 8, pp. 1129-1137, 2017.

[14] M. F. M. Arani and Y. A. R. I. Mohamed, "Dynamic Droop Control for Wind Turbines Participating in Primary Frequency Regulation in Microgrids," *IEEE Transactions on Smart Grid,* vol. PP, no. 99, pp. 1-1, 2017.

[15] F. Díaz-González, M. Hau, A. Sumper, and O. Gomis-Bellmunt, "Participation of wind power plants in system frequency control: Review of grid code requirements and control methods," *Renewable and Sustainable Energy Reviews,* vol. 34, pp. 551-564, 2014/06/01/ 2014.

[16] L. Holdsworth, J. B. Ekanayake, and N. Jenkins, "Power system frequency response from fixed speed and doubly fed induction generator‐based wind turbines," *Wind Energy: An International Journal for Progress and Applications in Wind Power Conversion Technology,* vol. 7, no. 1, pp. 21-35, 2004.

[17] M. F. M. Arani and Y. A. R. I. Mohamed, "Analysis and Impacts of Implementing Droop Control in DFIG-Based Wind Turbines on Microgrid/Weak-Grid Stability," *IEEE Transactions on Power Systems,* vol. 30, no. 1, pp. 385-396, 2015.

[18] O. Anaya-Lara, F. Hughes, N. Jenkins, and G. Strbac, "Contribution of DFIG-based wind farms to power system short-term frequency regulation," *IEE Proceedings-Generation, Transmission and Distribution,* vol. 153, no. 2, pp. 164-170, 2006.

[19] Z. Wu, W. Gao, J. Wang, and S. Gu, "A coordinated primary frequency regulation from Permanent Magnet Synchronous Wind Turbine Generation," in *2012 IEEE Power Electronics and Machines in Wind Applications*, 2012, pp. 1-6.

[20] J. N. Sakamuri, M. Altin, A. D. Hansen, and N. A. Cutululis, "Coordinated frequency control from offshore wind power plants connected to multi terminal DC system considering wind speed variation," *IET Renewable Power Generation,* vol. 11, no. 8, pp. 1226-1236, 2017.

[21] B. Silva, C. Moreira, L. Seca, Y. Phulpin, and J. P. Lopes, "Provision of inertial and primary frequency control services using offshore multiterminal HVDC networks," *IEEE Transactions on Sustainable Energy,* vol. 3, no. 4, pp. 800-808, 2012.

[22] C. Li, P. Zhan, J. Wen, M. Yao, N. Li, and W. J. Lee, "Offshore Wind Farm Integration and Frequency Support Control Utilizing Hybrid Multiterminal HVDC Transmission," *IEEE Transactions on Industry Applications,* vol. 50, no. 4, pp. 2788-2797, 2014.

[23] A. Junyent-Ferr, Y. Pipelzadeh, and T. C. Green, "Blending HVDC-link energy storage and offshore wind turbine inertia for fast frequency response," *IEEE Transactions on sustainable energy,* vol. 6, no. 3, pp. 1059-1066, 2015.

[24] H. Liu and Z. Chen, "Contribution of VSC-HVDC to Frequency Regulation of Power Systems With Offshore Wind Generation," *IEEE Transactions on Energy Conversion,* vol. 30, no. 3, pp. 918-926, 2015.

[25] I. M. Sanz, B. Chaudhuri, and G. Strbac, "Inertial response from offshore wind farms connected through DC grids," *IEEE Trans. Power Syst,* vol. 30, no. 3, pp. 1518-1527, 2015.

[26] Y. Li, Z. Xu, J. Østergaard, and D. J. Hill, "Coordinated Control Strategies for Offshore Wind Farm Integration via VSC-HVDC for System Frequency Support," *IEEE Transactions on Energy Conversion,* vol. 32, no. 3, pp. 843-856, 2017.

[27] Y. Li and Z. Xu, "Coordinated Control of Wind Farms and MTDC Grids for System Frequency Support," *Electric Power Components and Systems,* vol. 45, no. 4, pp. 451-464, 2017/02/25 2017.

[28] A. B. T. Attya and J. L. Dominguez-García, "Insights on the provision of frequency support by wind power and the impact on energy systems," *IEEE Transactions on Sustainable Energy,* vol. 9, no. 2, pp. 719-728, 2018.

[29] S. G. Vennelaganti and N. R. Chaudhuri, "Ratio-based Selective Inertial and Primary Frequency Support through MTDC Grids with Offshore Wind Farms," *IEEE Transactions on Power Systems,* 2018.

[30] A. E. Leon, "Short-term frequency regulation and inertia emulation using an MMC-based MTDC system," *IEEE Transactions on Power Systems,* vol. 33, no. 3, pp. 2854-2863, 2018.

[31] F. D. Bianchi and J. L. Domnguez-Garca, "Coordinated Frequency Control Using MT-HVDC Grids With Wind Power Plants," *IEEE Transactions on Sustainable Energy,* vol. 7, no. 1, pp. 213-220, 2016.

[32] S. Heier, "Grid integration of wind energy conversion systems, 1998," *ISBN 0,* vol. 471, p. 97143, 2002.

[33] R. Pena, J. C. Clare, and G. M. Asher, "A doubly fed induction generator using back-to-back PWM converters supplying an isolated load from a variable speed wind turbine," *IEE Proceedings - Electric Power Applications,* vol. 143, no. 5, pp. 380-387, 1996.

[34] N. W. Miller, J. J. Sanchez-Gasca, W. W. Price, and R. W. Delmerico, "Dynamic modeling of GE 1.5 and 3.6 MW wind turbine-generators for stability simulations," in *2003 IEEE Power Engineering Society General Meeting (IEEE Cat. No.03CH37491)*, 2003, vol. 3, pp. 1977-1983 Vol. 3.

[35] N. W. Miller, W. W. Price, and J. J. Sanchez-Gasca, "Dynamic modeling of GE 1.5 and 3.6 wind turbine-generators," *GE-Power systems energy consulting,* no. 3.0, 2003.

[36] N. A. Orlando, M. Liserre, R. A. Mastromauro, and A. Dell'Aquila, "A survey of control issues in PMSG-based small wind-turbine systems," *IEEE transactions on*

Industrial Informatics, vol. 9, no. 3, pp. 1211-1221, 2013.
[37] V. Akhmatov, *Induction generators for wind power*. Multi-Science Pub., 2005.
[38] L. Yang, Z. Xu, J. Ostergaard, Z. Y. Dong, and K. P. Wong, "Advanced control strategy of DFIG wind turbines for power system fault ride through," *IEEE Transactions on power systems,* vol. 27, no. 2, pp. 713-722, 2012.
[39] Y. Wang, H. Bayem, M. Giralt-Devant, V. Silva, X. Guillaud, and B. Francois, "Methods for Assessing Available Wind Primary Power Reserve," *IEEE Transactions on Sustainable Energy,* vol. 6, no. 1, pp. 272-280, 2015.
[40] A. Buckspan, L. Pao, J. Aho, and P. Fleming, "Stability analysis of a wind turbine active power control system," in *2013 American Control Conference*, 2013, pp. 1418-1423.
[41] Z. S. Zhang, Y. Z. Sun, J. Lin, and G. J. Li, "Coordinated frequency regulation by doubly fed induction generator-based wind power plants," *IET Renewable Power Generation,* vol. 6, no. 1, pp. 38-47, 2012.
[42] A. Koerber and R. King, "Combined Feedback-Feedforward Control of Wind Turbines Using State-Constrained Model Predictive Control," *IEEE Transactions on Control Systems Technology,* vol. 21, no. 4, pp. 1117-1128, 2013.
[43] P. Kundur, N. J. Balu, and M. G. Lauby, *Power system stability and control*. McGraw-hill New York, 1994.
[44] I. Report, "Dynamic models for steam and hydro turbines in power system studies," *IEEE Transactions on Power Apparatus and Systems,* no. 6, pp. 1904-1915, 1973.
[45] "DTU Database on Wind Characteristics," http://www.winddata.com/, accessed on 10 May 2014.